20th Australasian Fluid Mechanics Conference

Perth, Australia

5-8 December 2016

A dominant near-inertial internal wave field on the Tasmanian Continental Shelf

T.L. Schlosser[1], N.L. Jones[1], C.E. Bluteau[1], A.J. Lucas[2] and G. Ivey[1]

[1]School of Civil, Environmental and Mining Engineering & Oceans Institute
University of Western Australia, Crawley 6009, Australia

[2]Scripps Institution of Oceanography
University of California, San Diego, La Jolla, CA, USA

Abstract

The Tasmanian Eastern Continental Shelf (TECS) has a complex internal wave field forced by surface tides and wind. To quantify these flow fields, we deployed three traditional moorings and two autonomous profilers on a transect across the relatively narrow shelf for 18 days in February 2015. These moorings provided temperature and velocity measurements through the water column. Harmonic analysis of the observed velocities indicates that time varying near-inertial waves are an order of magnitude more energetic than internal tides and dominate the internal wave field. We link variations in near-inertial wave velocities to variations in the surface wind stress.

Introduction

Internal waves are a ubiquitous physical process on density-stratified continental shelves. Internal waves can transport nutrients and other tracers vertically and horizontally, through mixing and nonlinear advective processes, thereby modifying the primary productivity of coastal waters [4, 6]. These baroclinic (depth-varying) processes can be generated by the barotropic (depth-constant) tides, the wind and other processes. When the barotropic tide forces stratified water vertically over topography, tidally-forced internal waves originate from the seabed, called the internal tide [5]. In contrast, wind-forced internal waves originate at the water-surface [8]. Their frequency is generally similar to the Coriolis frequency (i.e. near-inertial) and when freely propagating we call them near-inertial internal waves (NIW) [2]. The internal wave field of a continental shelf is thus dependent on the local wind and tide forcing, as well as remotely generated internal waves that propagate on the shelf.

Here we present field observations on the TECS of the internal wave field and the barotropic tide and wind that force this internal wave field. The internal wave field of this shelf has many unique features and is vastly unstudied, despite widespread evidence of the importance of internal waves to the physical and biological dynamics of continental shelves. The TECS experiences strong and variable winds and its barotropic tidal range is around 1.4 m. One of the world's most energetic internal wave beams also propagates across the Tasman Sea to the Tasman Continental Slope [11], which we originally expected transferred significant energy to the shelf through internal waves at the tidal frequency. Instead, we show that NIWs dominate the internal wave field at this site and are coherent with the local wind field in the upper water column.

Methods

Study Site

Our study site is in the north-east of the TECS at 41.1°S, where the shelf is 28 km wide and its depth gradually increases to 200 m at the shelf-break (figure 1a). The continental slope is orientated approximately north-south at an angle of 3° to the east. The inertial period at this latitude is 18.1 h. Tasmania lies in the path of the 'Roaring Forties' and therefore experiences considerable periods of strong westerly winds. The northern limit of the westerly wind belt is commonly approximately 40°S in winter months and 44°S in summer months [13]. The Bureau of Meteorology St Helens station has been in operation since 2001. The Austral summer winds from St Helens are predominantly towards the north or south, but are strong and variable. During the Austral summer months the East Australian Current (EAC) Extension commonly ranges to approximately 42°S [10]. The EAC Extension transports warm and salty tropical water south from north-eastern Australia to the cool temperate waters of the TECS. An undercurrent transports colder water northwards, with reduced flow volumes compared to the EAC Extension. We expect this combination of tide, wind and mesoscale processes will result in a complex shelf response.

Field Measurements

In total, we deployed six moorings on the TECS for 18 days in February 2015. However, we present only the measurements from one of the autonomous profilers (WireWalker), deployed at 148.5357°E, 41.3854°S, in 114 m of water. We co-located this profiler with a bottom-fixed acoustic Doppler current profiler (ADCP, RDInstruments 300 kHz Workhorse). The ADCP measured pressure, in addition to velocities in 2 m vertical bins that ensemble-averaged 6 pings per ensemble in 10 second intervals. We quality controlled and time-averaged these measurements to 2 minute time intervals. The autonomous profiler sampled the entire water-column approximately every 8 minutes, with a vertical resolution of 25 cm [7]. It measured temperature and salinity in addition to other physical and biological variables.

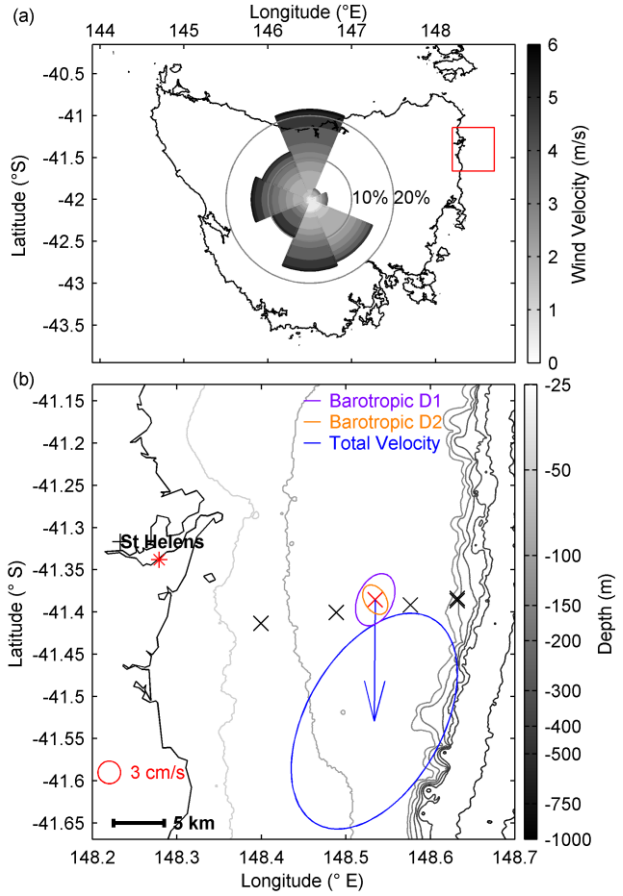

Figure 1: (a) Tasmania, Australia, with study site indicated by a red square. Wind rose for month of February 2015 recorded at St Helens (red asterisk in b); the direction indicates the direction the wind is blowing towards. (b) Map of the local bathymetry and mooring locations (crosses). Our paper focuses on the autonomous profiler (red cross). The arrow indicates mean flow velocity and ellipses indicate flow velocity of one standard deviation along the major and minor axis of flow direction.

Data Analysis

We analysed the measured velocity timeseries from the ADCP collocated with the autonomous profiler. The barotropic flow is depth- and density-independent, which we approximate as the depth-averaged velocity. To derive the baroclinic velocities, we subtracted the depth-averaged velocity from the total velocity. We have assumed all wave-like motions at the near-inertial frequency are freely propagating internal-gravity waves. We performed harmonic analysis on the baroclinic velocities at the diurnal (D1), semidiurnal (D2) and inertial frequencies. A sliding harmonic fit was performed on segments of 3 days, with segments overlapping by all but one time step. We derived a signal-to-noise ratio for all time segments from the harmonic fit and residual time series and discarded time segments with a signal-to-noise ratio less than three. For each time step, we then averaged harmonic amplitudes of the remaining overlapping time segments. By reducing the segment lengths to 3 days, our harmonic analysis could only separate the semidiurnal ($\omega \sim 2$ cycles per day), near-inertial, and diurnal frequencies ($\omega \sim 1$ cycle per day) from each other but not the individual constituents such as the S2 and M2. Therefore, we use D1 to denote the diurnal K1 and O1 tidal constituents and D2 to denote the semidiurnal M2 and S2 constituents. Through harmonic analysis, we have isolated the tidal and near-inertial baroclinic variations over time and depth.

We calculated the horizontal kinetic energy (HKE) using:

$$HKE = \int_{-H}^{0} \frac{1}{2}\rho|\boldsymbol{u}_{bc}|^2 dz \quad \text{.....(1)}$$

Here ρ is the water density from the autonomous profiler's measurements, H is the water depth (114 m) and $\boldsymbol{u}_{bc}$ is the baroclinic velocity. Bold variables indicate a vector quantity, including both cross- and along-shore components. We use a depth varying 60-h low-pass filtered water density for our HKE calculations.

We calculated the wind stress using:

$$\boldsymbol{\tau_w} = C_D \rho \boldsymbol{v}|\boldsymbol{v}| \quad \text{.....(2)}$$

Here $\boldsymbol{v}$ is the wind velocity; C_D is the drag coefficient, estimated at 1.4×10^{-3} and ρ is the air density estimated at 1.2 kgm^{-3}.

Rotary spectra is a method of separating vector quantities by their rotation direction, where NIWs rotate cyclonically or counter-clockwise in the Southern hemisphere. We quantitatively compare the coherence of the wind stress and the water velocities via cross-spectra of the rotary spectra. We compare only the cyclonic components of the wind stress and water velocities. We use the sine-multitaper method [1, 9], which preserves the low frequency range. The form of the rotary spectra was given by:

$$\hat{S}(\omega) = \Delta t \left| \sum_{t=1}^{N} w_t \boldsymbol{u}_{bc} e^{-i2\pi\omega\Delta t} \right|^2 \quad \text{.....(3)}$$

Where w_t is the window function as per the sine-multitaper method, ω is the frequency, and Δt is the sampling interval. The term $\boldsymbol{u}_{bc}$ can also be replaced by $\boldsymbol{\tau_w}$. We use equation 5.205 (p.518) in Thompson and Emery [12] to calculate the inner cross spectra between the wind stress and baroclinic velocities rotating in the same direction, defined as $\hat{S}^{+}_{\tau_w u_{bc}}$ for $\omega > 0$ (cyclonic).

Results and Discussion

Background Conditions

Over the entire 18-day record, the EAC Extension flowed southward (blue arrow in figure 1b). The total (barotropic and baroclinic) velocities flowed generally southwards at 14 cms^{-1}. During the month of our measurements, measured winds from St Helens were directed predominantly in the north and south directions (along-shore, figure 1a). Our shipboard wind measurements, which we use to calculate wind stress in figure 2b, showed that the wind blew in a similar direction compared with the St Helens' station. We use the shipboard winds for wind stress as the ship was generally closer to the mooring site.

To separate the dominant tidal constituents, we performed harmonic analysis of the water surface elevation, measured by the bottom-mounted ADCPs pressure sensor. The four most dominant constituents were, in order of reduced influence, the semidiurnal M2, the diurnal K1, O1 and the semidiurnal S2, with maximum surface elevations of 35 cm, 12 cm, 8 cm and 7 cm, respectively. Neap tide is on day 42 and the spring tide is on day 49. The stratification was relatively strong with a buoyancy period of about 1 min up to day 49, when the stratification weakened and the buoyancy period increased to 2 min (not shown). For the entire field campaign, the stratification supported internal waves.

TECS Internal Wave Field

Barotropic tidal velocities were significantly stronger than their respective baroclinic velocities; however, the near-inertial baroclinic velocities at times exceeded the barotropic tidal velocities. Barotropic tidal velocities reached 11 cms^{-1} and averaged 5 cms^{-1} over the measurement period (figure 2a). The median and 95th percentile baroclinic tidal velocities were around 2.4 cms^{-1} and 4.3 cms^{-1}, respectively, for both D1 and D2 (not

shown). At this site, little energy was evident from the externally generated M2 tidal beam that propagates onto the Continental Slope from across the Tasman Sea. The baroclinic NIW velocities were significantly stronger with median and 95th percentile magnitudes of 3.4 cms^{-1} and 9.1 cms^{-1}, respectively (figure 2d). The NIW baroclinic velocities were strongest near the surface, averaging 6.9 cms^{-1}, while those mid-depths and near the bottom averaged at 3.5 cms^{-1} and 3.0 cms^{-1}, respectively (figure 2d). These near-bottom averages, although half of near-surface estimates, were still larger than the median near-bottom baroclinic tidal velocities. The mean and maximum baroclinic NIW velocities therefore exceeded the baroclinic tidal velocities.

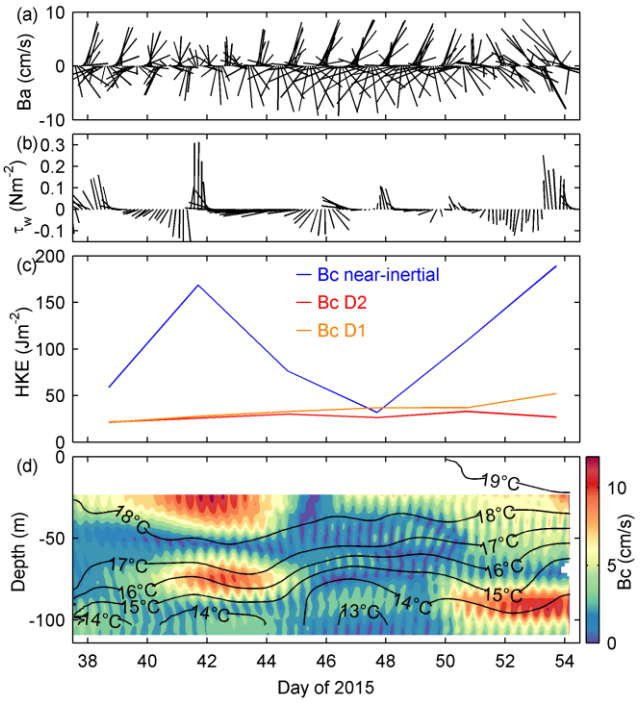

Figure 2: (a) Barotropic velocities at all tidal frequencies, (b) wind stress 6-hour low-pass filtered, (c) depth-integrated horizontal kinetic energy (HKE) of baroclinic velocities at labelled frequency, and (d) baroclinic velocity magnitude (cross and along-shore) at near-inertial frequency. In (d) the 60-h low-pass filtered isotherms(°C) are shown in black. Arrow direction in a-b is geographical (i.e. up is north, left is west).

The HKE conveys the proportion of energy in the different frequencies (figure 2c). The baroclinic tidal velocities had similar magnitudes throughout the 18 days, resulting in a nearly constant HKE with a mean of 35 Jm^{-2}. In contrast, the NIW HKE varied by an order of magnitude (80 Jm^{-2}) over 4 day periods. This highlights the baroclinic near-inertial signal is temporally variable, due to the non-stationarity of the wind-forcing and other dynamics to be explored in future work. The mean HKE of the baroclinic NIW was 106 Jm^{-2}, an order of magnitude larger than that of the baroclinic tides. We conclude that NIWs were the most dominant baroclinic motion on TECS during our field campaign.

The rotary coefficient describes both the rotation direction through its sign (clockwise or counter-clockwise) and the degree of rotation versus unidirectional flow. A value of one represents perfect cyclonic circles (counter-clockwise) and zero represents unidirectional flow. We computed the rotary coefficient from the horizontal baroclinic harmonic analysis velocities. The rotary coefficient was close to one for most of the water-column, with a smaller coefficient at approximately mid-depth and close to the seabed (figure 3). A rotary coefficient of one is consistent with theory, which describes that waves become more circular as their frequency approaches the inertial frequency. We considered only horizontal flow, but rotary coefficients less than one indicates there may be vertical propagation [3]. The NIW field therefore rotates cyclonically due to the Earth's rotation and is not limited to surface waters.

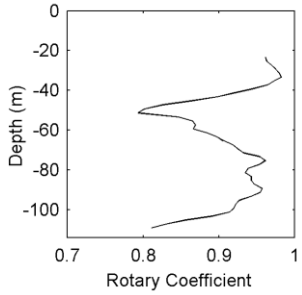

Figure 3: Rotary coefficient for baroclinic velocities at near-inertial frequency, calculated from harmonic analysis velocities. A value of one indicates perfectly circular, cyclonic (counter-clockwise) rotation.

Relating Wind and Bottom Stress to Near-Inertial Waves

We relate the observed NIW near the surface to the local winds by comparing the induced baroclinic velocity magnitudes in figure 2d with the wind stress in figure 2b. Large wind stresses that exist for less than the near-inertial period (18 h) and rotate cyclonically are most effective in creating NIW [8]. Winds rotated cyclonically and exceeded 0.2 Nm^{-2} on two occasions: day 41 and 53. Following these two large wind events, the near-surface NIW velocities increased to over 12 cms^{-1} and reached their maximum values over the record. Cyclonically rotating winds with magnitudes around 0.1 Nm^{-2} occurred more frequently; following these smaller wind stresses a weaker NIW response was recorded, with velocities around 6 cms^{-1} (day 38, 46 and 47). It is likely the near-surface NIW velocities on days 41 and 53 were larger due to the added influence of these prior, smaller wind events as there is little evidence of velocities decreasing in the mixed layer before the larger wind events. From day 43 to 45 winds were sustained at over 0.1 Nm^{-2} and blew westwards (aligned along x-axis). After these sustained winds the near-surface NIW velocities were their smallest over the whole record. We attribute these small velocities to the wind blowing for over two inertial periods and emphasise that efficient generation of NIWs requires not only strong winds that rotate cyclonically, but also winds that periodically relax with a frequency near or less than the Coriolis frequency [8].

The NIW velocity structure at depth is complex. Velocities over 6 cms^{-1} occurred at depths over 50 m deep during large wind stresses (>0.1 Nm^{-2}) for days 41-44, but not days 50-54 (figure 2d). On days 46 and 47, the near-surface NIW velocities were smaller; however, there were four isolated depth layers with velocities over 5 cms^{-1}. On days 41-44, the thermocline's stratification is stronger at 1 min period and corresponded approximately to the 16°C isotherm. During this period, the large NIW velocities at depth do not penetrate the thermocline. After day 50 the thermocline weakens to 1.5 min period and decreases to a depth of 90 m on day 50 (~14°C isotherm), then sharply rises to 50 m on day 53 (~16°C isotherm). We attribute the large velocities on days 50-54 penetrating to depths of 90 m, below the 16°C isotherm to the weakening in the thermocline's stratification. There were also additional periods where NIW velocities exceeded 5 cms^{-1} at depths below the thermocline. We then statistically compare the wind field to the water velocities through cross spectra.

Inner cross rotary spectra of the cyclonic wind stress and water velocities revealed the coherence of the two signals, their time

lag and the energy at certain frequencies. We compare the wind stress to the water velocities at two depths. Near the surface, water velocities were coherent with the wind at the near-inertial frequency (figure 4a), with a phase difference of approximately 32° or 1.6 hours with water lagging wind (figure 4b). This confirms the qualitative relationship explored above between the wind stress and NIW velocities in figure 2. The velocities at depth were also coherent with the wind at the near-inertial frequency, however the baroclinic velocities were less coherent and the variance shared with the wind was weaker at this depth (figure 4c-d). The phase difference was approximately -155° (335°) or -7.8 hours (16.8 hours). For both depths, the inner cross spectra shows the wind energises all frequencies, with the greatest response at the inertial frequency, as found by other studies [8].

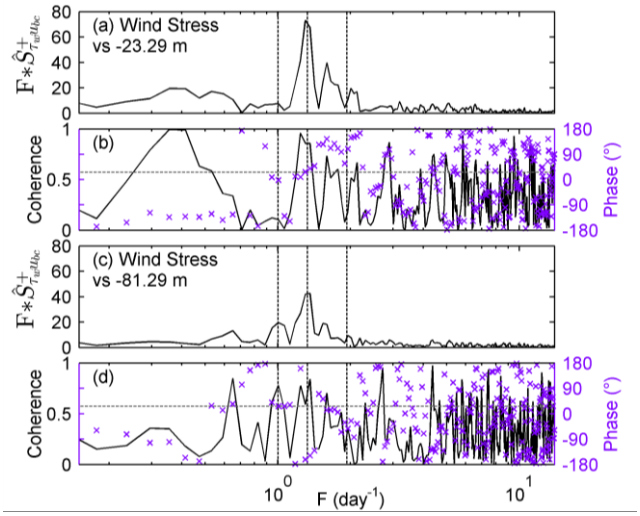

Figure 4: Inner cross-spectra of cyclonic (counter-clockwise) shipboard wind stress and baroclinic water velocities at 23 m (a-b) and 81 m (c-d) depth. Horizontal dashed lines in b and d show the 95% significance and all vertical dashed lines mark the diurnal, inertial and semidiurnal frequencies. Positive phase indicates the wind leads the currents and vice versa.

Conclusions

The TECS field observations demonstrate that NIWs dominate the internal wave field. The local wind forced the near-surface NIW, as revealed by a comparison of NIW velocities with the local wind stress. Large wind stresses that were sustained for less than one inertial period (18 hours) and rotated cyclonically appeared to be most effective at generating NIWs, which also rotate cyclonically in circular motions throughout the water-column. The local wind stress was significantly coherent with the water velocities at the near-inertial frequency, although the coherence of the signal weakened with increasing depth. This suggests other factors were influencing the NIW field at depth, which requires further analysis.

A more detailed analysis of the NIW dynamics will be the focus of future work. This work will include an energy balance, the energy flux variations and the modal separation of NIW on the TECS. Spatial variations will be analysed across the shelf using the physical measurements from five other moorings. Our ultimate goal is to link the NIWs physical dynamics to the biological response on the shelf.

Acknowledgements

This work was funded by an Australian Research Council Discovery Project (DP 140101322), a UWA Research Collaboration Award and a UWA ECM Research Development Award. We acknowledge the anonymous reviewer whose detailed comments improved the quality of this work. T. L. Schlosser acknowledges the support of a University Postgraduate Award. We also acknowledge the crew of the R/V Revelle and Chief Scientist Professor Rob Pinkel.

References

[1] Alford, M.H., & Whitmont, M., Seasonal and Spatial Variability of Near-Inertial Kinetic Energy from Historical Moored Velocity Records. *J. Phys. Oceanogr.*, **37**, 2007, 2022–2037.

[2] D'Asaro, E.A., The Energy Flux from the Wind to Near-Inertial Motions in the Surface Mixed Layer. *J. Phys. Oceanogr.*, **15**, 1985, 1043–1059.

[3] Kundu, P.K., An Analysis of Inertial Oscillations Observed Wear Oregon Coast. *J. Phys. Oceanogr.*,1976.

[4] Leichter, J., Shellenbarger, G., Genovese, S.J., & Wing, S., Breaking internal waves on a Florida (USA) coral reef:a plankton pump at work? *Mar. Ecol. Prog. Ser.*, **166**, 1998, 83–97.

[5] Lim, K., Ivey, G.N., & Jones, N.L., Experiments on the generation of internal waves over continental shelf topography. *J. Fluid Mech.*, **663**, 2010, 385–400.

[6] Lucas, A.J., Franks, P.J.S., & Dupont, C.L., Horizontal internal-tide fluxes support elevated phytoplankton productivity over the inner continental shelf. *Limnol. Oceanogr. Fluids Environ.*, **1**, 2011, 56–74.

[7] Pinkel, R., Goldin, M.A., Smith, J.A., Sun, O.M., Aja, A.A., Bui, M.N., & Hughen, T., The Wirewalker: A vertically profiling instrument carrier powered by ocean waves. *J. Atmos. Ocean. Technol.*, **28**, 2011, 426–435.

[8] Pollard, R.T., On the generation by winds of inertial waves in the ocean. *Deep Sea Res. Oceanogr. Abstr.*, **17**, 1970, 795–812.

[9] Rayson, M.D., Ivey, G.N., Jones, N.L., Lowe, R.J., Wake, G.W., & McConochie, J.D., Near-inertial ocean response to tropical cyclone forcing on the Australian North-West Shelf. *J. Geophys. Res. Ocean.*, **120**, 2015, 7722–7751.

[10] Ridgway, K.R., Long-term trend and decadal variability of the southward penetration of the East Australian Current. *Geophys. Res. Lett.*, **34**, 2007, 1–5.

[11] Simmons, H.L., & Alford, M.H., Simulating the Long-Range Swell of Internal Waves Generated by Ocean Storms. *Oceanography*, **25**, 2012, 30–41.

[12] Thomson, R.E., & Emery, W.J., *Data Analysis Methods in Physical Oceanography*. Newnes, 2014.

[13] Wyrtki, K., *The Surface Circulation in the Coral and Tasman Seas*. Melbourne1960.